SCANNING TUNNELING MICROSCOPY (STM) INDUCED GRAPHENE NANORIBBON (GNR) SYNTHESIS

BY

STEVEN KOLACZKOWSKI

THESIS

Submitted in partial fulfillment of the requirements
for the degree of Bachelor of Science in Electrical Engineering
in the Engineering College of the
University of Illinois at Urbana-Champaign, 2019

Urbana, Illinois

Adviser:

Professor Joseph Lyding

ABSTRACT

Graphene, a monoatomic layer of hexagonal lattice carbon, has been of interest to researchers in recent years due to its environmentally dependent band structure, its optical properties, and its potential device applications. However, since graphene in its natural, flat state is metallic, sheets of graphene are not good candidates for creating transistors. But, when laterally confined to a few carbon atoms across, graphene becomes semiconducting depending on the size and shape of the confinement. These structures are called graphene nanoribbons or GNRs. GNR synthesis is currently done in solution or thermally on a substrate covered with bromoaromatic precursors. While both of these methods produce large amounts of atomically precise GNRs, when viewed on a surface, they lack uniformity in length, spacing, and orientation. This paper shows the ability to use ultra-high vacuum scanning tunneling microscopy (UHV-STM) to spatially control the polymerization of 10,10-dibromo-9,9-bianthracene (DBBA), the 7A GNR precursor, into polyanthrylene (PA), the polymer formed in the 7A GNR synthesis process. Using this STM based polymerization allows precise control over the length, orientation, and spacing of the PA and, given future work, could lead to this same atomically precise growth of PA into 7A GNRs.

Subject Keywords: Graphene; Graphene nanoribbon; Scanning tunneling microscopy; Gold; Herring bone

To my family, for their love and support. And to my friends; without them distracting me, I would've finished this weeks ago and gone crazy years ago.

TABLE OF CONTENTS

LIST OF FIGURES

LIST OF ABBREVIATIONS

GNR	Graphene Nanoribbon
UHV	Ultra-High Vacuum
STM	Scanning Tunneling Microscopy or Scanning Tunneling Microscope
DBBA	10,10-dibromo-9,9-bianthracene
PA	Polyanthrylene
FET	Field Effect Transistor
GAAFET	Gate-all-around Field Effect Transistor
UV	Ultra Violet
DCT	Dry-Contact Transfer
Au	Gold
Si	Silicon
C	Carbon
Br	Bromine

CHAPTER 1

INTRODUCTION

1.1 Scanning Tunneling Microscopy (STM)

A scanning tunneling microscope operates by bringing an atomically sharpened tip within angstroms of a surface. The microscope electronics record the amount of electron tunneling current between the surface and sample. Tunneling current can be achieved by electrons tunneling either from tip to sample (corresponding to a positive sample bias) or from sample to tip (corresponding to a negative sample bias). The ability to control the potential difference between sample and tip allows the user to construct IV spectra data and density of states of the surface. When set to a constant-current mode scan (the mode used in this experiment), the tip will raster scan across the sample over a preset area and either approach or retract from the surface to maintain a constant tunneling current. This gives a combined topological and density of states characterization of the surface. STM can be operated at a variety of temperatures, including cryogenic, making it a useful tool for characterizing systems with unique emergent properties that only appear in specific temperature regimes. It is significant to note that resolution of scanning scales inversely with temperature. In this experiment we are operating at room temperature, so tip conditioning is a vital step to ensuring high resolution and the ability to accurately describe the scanned surface. More information on tip conditioning will be covered in Section 2.3. Another important characteristic of STM is that at sufficiently high tip-sample biases it has been shown that the tunneling current can be used to cleave individual atomic bonds on the surface of the material. This was first verified with atomic precision by desorbing hydrogen from the surface of Si(100) [1].

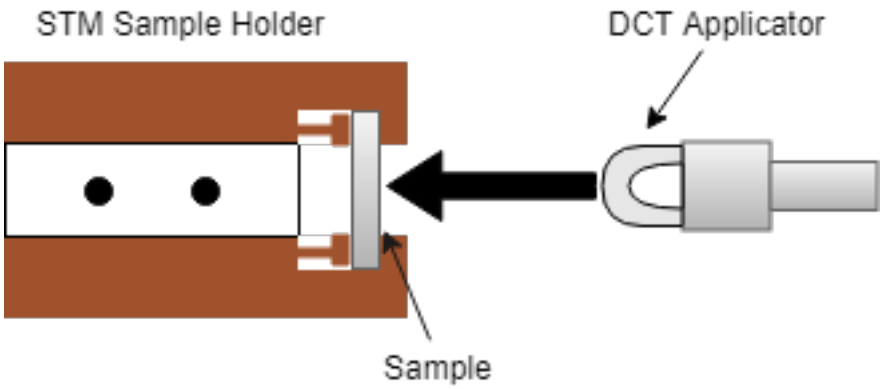

Figure 1.1: Dry Contact Transfer Process

1.2 Dry-Contact Transfer (DCT)

Dry-contact transfer is a method of transferring molecules to the surface of a sample under UHV developed by Professor Lyding [2]. The advantage of DCT is that it removes any solvents and desorbed gasses from the desired material and transfers in situ, not requiring the surface to be re-exposed to atmospheric pressure. DCT applicators are usually metallic frames with a fiberglass tip that is pressed into the sample surface, as shown in Fig. 1.1. A more detailed description of DCT applicator building will come in Section 2.2. The reason that DCT works as method of material transfer is that the bonds holding the material to the fiberglass are too weak to maintain when pressed against the sample surface.

1.3 2D Materials

With transistors reaching sizes of sub 7nm, silicon is reaching the limit of its ability to prevent leakage current from flowing through the gate oxide. In fact, most modern semiconductor processing companies eager to reach the 5nm node goal (set by the International Roadmap for Devices and Systems for 2020) have moved to alternate FET configurations including the FinFET and GAAFET. However, these configurations are not expected to be able to support Silicon processing of transistors below 4nm node lengths.

One promising way to circumvent this limit is through the use of 2D materials. 2D materials have the advantages of being atomically thin, have a wide

variety of bandgaps, and have unit cells that are confined to less than a few nanometers. For example, it has been demonstrated that MoS_2 can be used to build a transistor of 1nm gate length [3]. One such promising material is a confined structure of graphene, the graphene nanoribbon (GNR). Graphene nanoribbons have all the previously listed advantages of 2D materials, with the added benefits of carrier mobilities of order $10^3 - 10^5$ cm^2/Vs [4] and the ability to be fabricated with atomic precision without conventional lithographic methods.

1.4 GNR Synthesis

In the history of GNR synthesis both top-down lithographic and bottom-up methods have been investigated. Top-down methods have the advantage of using recipes similar to those used for years by modern industrial semiconductor processing companies. These processes utilize wet chemical etching and E-beam lithography to define the GNR structure. However, despite sub-10nm resolution achievable by E-beam lithography, this process is incapable of ensuring atomic precision in GNR edge construction. The band structure and carrier mobility of GNRs vary greatly with alterations to their edge states and, because of this, top-down GNR fabrication is currently infeasible.

However, within the last decade, great advances have been made in the field of bottom-up synthesis of GNRs. The most relevant to this thesis is the demonstration of atomically precise GNR synthesis through heating of monolayers of bromoaromatic monomers [5]. This synthesis is often performed on Au(111) surfaces because the surface states allow the precursor monomers to spread into a monolayer when annealed to approximately 100°C after deposition. This is often not a uniform monolayer across the entire substrate and rather forms 'islands' of precursor molecules. With the temperature raised to approximately 200°C the bromine-carbon bond is cleaved on the precursor molecules and neighboring monomers arrange to form long polymers. This process is often referred to in the literature as polymerization or dehalogenation and is facilitated by Ullmann coupling. Lastly, with the temperature raised even higher to approximately 400°C the polymer chains cyclodehydrogenate and form atomically precise GNRs. This was first demonstrated with the synthesis of the 7A and Chevron GNR from the 10,10-99- dibromo-

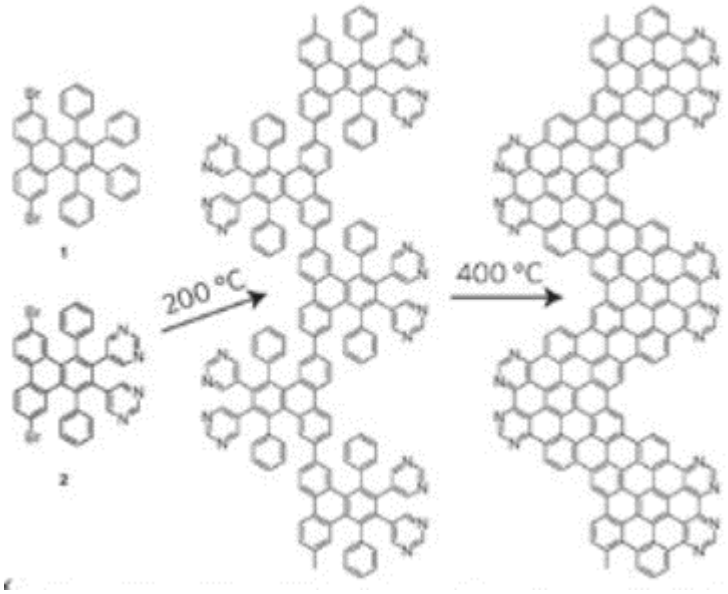

Figure 1.2: Chevron-N GNR Synthesis [6]

bianthryl (DBBA) and 6,11-dibromo-1,2,3,4-tetraphenyltriphenylene molecules respectively [5]. The chemical reaction mechanisms for chevron GNR synthesis is shown in Fig. 1.2

This procedure for GNR synthesis has been successful at producing dozens of different kinds of GNR structures. However, despite its consistent ability to produce atomically precise GNRs it has not led to wide-scale use of GNRs for device applications due to several inherent issues. One major issue is that, while gold is a wonderful material for synthesis of GNRs, as it is metallic, it cannot function as a substrate for GNR devices. This is due to the fact that any potential induced across a GNR on a gold substrate will allow orders of magnitude more current to flow through the substrate than the GNR itself. Secondly, this process is stochastic in nature and therefore does not allow for control over the length, orientation or spacing of the thermally formed GNRs. this is shown in Fig. 1.3. Lengths of GNRs can vary from several angstroms to tens of nanometers. GNRs on single substrate terraces have no clear preference in their angular distribution. Neighboring GNRs can be as close as touching and overlapping to several nanometers away (or even microns from their nearest neighbor depending on the precursor island size). This makes analyzing the electrical and thermal conductivity of GNRs and building GNR devices nearly impossible. With a random distribution of GNRs on a metallic surface, we cannot build electrical contacts to individual

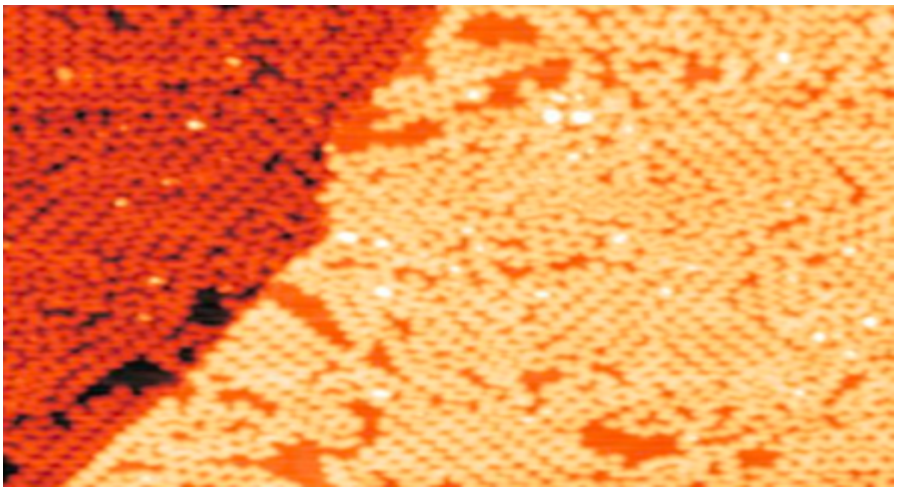

Figure 1.3: Chevron GNRs Synthesized on Au(111) Substrate through Stochastic, Thermal Processes [6]

GNRs in order to carry out this characterization. Some work has been done to help try and mitigate these problems. For instance, it has been shown that precursor molecule islands deposited near substrate terrace edges tend to form GNRs oriented in the same direction as the terrace edge. However, this limited angular preference is not enough to allow for reliable GNR contacts to be made [5].

In future chapters a method for forming GNRs through the same polymerization and cyclodehydorgenation steps with deterministic control of GNR length, orientation, and spacing is proposed. Additionally, the methods used to achieve such results and preliminary data in the experiment will be presented.

CHAPTER 2

METHODS

2.1 Proposal

In order to achieve spatial control over GNR synthesis, we will utilize the STM's ability to tunnel electrons with atomic precision to a substrate. The STM tip will be used to selectively dehalogenate the precursor monomers and form polymer chains only where the STM tip has 'written'. This is possible because the bromine-carbon bond in the aromatic monomers is the weakest. A great advantage to 'writing' GNRs is it combines the determinism of top-down fabrication processes with the atomic precision of bottom-up natural processes. In this paper, polymerization of DBBA into PA will be discussed.

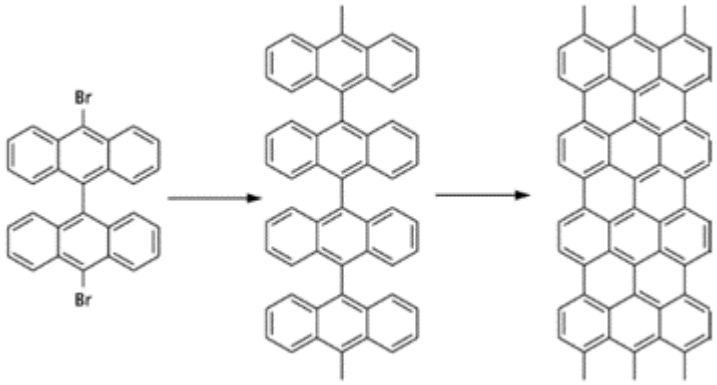

Figure 2.1: 7A GRN Synthesis. DBBA→PA→7A GNR [7]

Figure 2.2: STM Sample-holder with Au(111) Surface and Si Backing

2.2 Sample Preparation

2.2.1 Au(111) Substrate

In order to create a clean, functional environment for the polymerization of DBBA to occur we must take several steps to shape, support, and purify our sample surface. We began with a 1cm x 1cm square of 200nm thick Au(111) on mica substrate. This is trimmed to the size needed to fit into the STM sample holder. This gold portion is then heated under a hydrogen flame to resurface and ensure a (111) crystal pattern. The gold is then UV-ozone treated for 15mins to remove any remaining organic compounds from the surface. The gold sample is secured in the STM sample holder with a similarly sized silicon sample behind it (the silicon should be sprayed with acetone, isopropyl alcohol, deionized water, and isopropyl alcohol again to ensure there is no dust on the surface). This gives the thin gold sample mechanical support as well as a path for current to flow for heating purposes in UHV.

Once fully assembled the STM sample holder is transferred to UHV (P$\approx 1 * 10^{-10}$torr) and annealed at 150°C overnight. It is important that the sample is above 100°C to ensure any gasses or water on the surface desorbs, but below 200°C to avoid the thin gold surface pealing from the mica. The STM sample holder is then transferred to the STM and is ready for surface characterization and DCT of precursor molecules.

Figure 2.3: DCT Applicator

2.2.2 DBBA Applicator

The DBBA applicator is constructed out of a STM tip holder, short fiberglass tube, and thin stainless steel strip. To ensure that the metallic portions of the applicator are clean, they should be placed in an ultrasonic cleaner for fifteen-minute increments while submerged in acetone, isopropyl alcohol, deionized water, and isopropyl alcohol again. Once washed, these pieces are dried using compressed N_2. One side of the stainless steel strip should be spot-welded to the bottom of the tip holder. The fiberglass tube should then be sized such that it fits over the stainless steel, leaving enough at the end to be spot welded to the top of the tip holder. After spot welding the remaining loose end of stainless steel to the top of the tip holder, additional stainless steel may be spot welded to the edges of the fiberglass to avoid fraying. Once completed, the applicator should resemble that shown in Fig.2.3

A few milligrams of DBBA powder is then deposited into a container and the applicator is applied to the powder until a visible amount of the powder has transferred to the applicator. The applicator is now ready to be transferred to UHV and degassed. The applicator should be heated in UHV to approximately 150°C overnight to desorb any moister or gasses from the surface. If the temperature is too high, the DBBA will also sublime and not be available for the DCT process. Once this has been completed, the applicator is clean and ready for DCT onto the STM sample. If the material being DCT'd has a lower vapor pressure at high temperatures (like full GNRs), then it is recommended to degas to 350°-500°, as this will ensure any solvents on the applicator evaporate.

2.3 STM Scanning and Data Collection

During STM scanning and data collection, parameters such as tip-sample bias, tunneling current, scan size, scan location, and XYZ verniers may be adjusted. As these parameters change, the condition of the STM tip is altered and allows for greater or worse scan resolution. For example, if the tip is scanning over an area with lots of hills, valleys, or contaminants, the tip may crash into the surface and lose resolution. Alternatively, bringing the STM tip into tunneling range under high tip-sample bias may help eject contaminants off of the tip, improving resolution. Many tip altering methods and tip-sample biases used to improve resolution are surface dependant. Since our Au(111) surface is metallic, tunneling current will exist at any tip-sample bias. This has the advantage of being able to scan at low voltages, $\mid V \mid \leq 0.3V$ allowing us to scan without electrically activating any surface states. However, this also means that tip conditioning techniques that are well established for surfaces like Si(100) do not transfer to a Au(111) surface. Altering the tunneling current of the constant-current scan changes the relative distance between sample surface and tip. It has been shown that DBBA on a Au(111) surface will not react to an STM scan conducted at a sample-tip bias of -2.0V, but that DBBA will begin to debrominate when scanned at +2.0V [8]. This means that after DCT, the Au(111) sample should only be scanned at negative biases to avoid unintentional polymerization of deposited DBBA molecules. Similarly, IV spectra, which usually sweeps tip-sample bias from $\pm 2.0V$ may be conducted in regions where users are confident no DBBA exists or after DBBA polymerization, but should be avoided in DBBA dense regions.

CHAPTER 3

RESULTS AND DATA

3.1 Surface Characterization

When performing STM experiments, it is critical that the surface be well characterized. Even if studying a diffuse molecule placed on the surface, surface characterization provides a reference for microscope resolution and spectra data. The signature structure of Au(111) surfaces is called the herringbone reconstruction, a zig-zagging or alternating pattern that has a 5-10nm periodicity as shown in Fig. 3.1 and Fig. 3.2. If the STM scan is able to identify herringbone reconstruction, this implies that the tip-surface resolution is sufficient to collect data on properties like density of states, IV spectra, and topology of any features on the surface. This does not guarantee that there will be no error in these calculations; for example, tip-oxide formation may cause the bandgap to appear larger than expected with no effect on resolution. Therefore, once this resolution has been achieved, it is important to ensure that IV spectra data collection is also calibrated properly.

As Au(111) is metallic, there should be no bandgap when the spectrum is calculated. Since tunneling current varies exponentially with distance from sample, the current is amplified and recorded on a logarithmic scale. As shown in Fig. 3.3 this semilog IV spectrum corresponds to a linear response to external bias. The multiple curves represent the data collected at 50 different points on the gold surface. This data needs to be reconfirmed each time an STM tip is replaced. However, as this data is a function of both tip and sample purity, it does confirm the cleanliness and surface structure of the Au(111) which should remain constant across tip changes. Once this data has been collected, the surface is ready for DCT and scanning for DBBA molecule islands on the Au(111) surface can begin. This DCT process may also introduce fiberglass or other kinds of contaminants to the surface. These

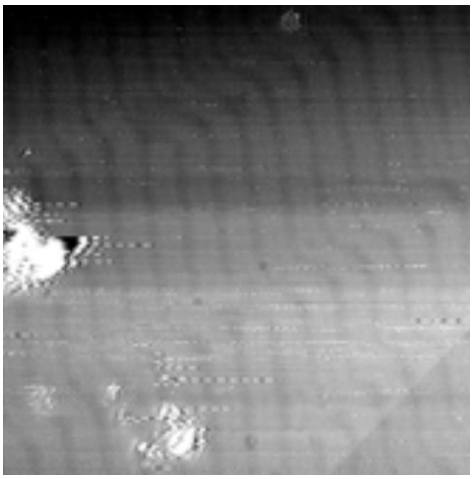

Figure 3.1: Au(111) Surface 600$\AA$ x 600$\AA$, +0.3V 0.1nA Scan, Herring Bone Reconstruction with 5.6nm Periodicity

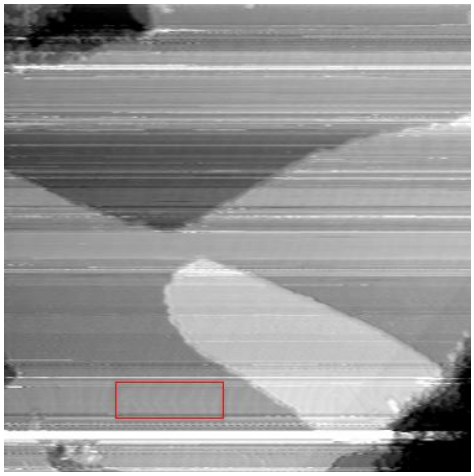

Figure 3.2: Au(111) Surface; 1200$\AA$ x 1200$\AA$, +0.3V, 0.1nA Scan; Herring Bone in Red Box

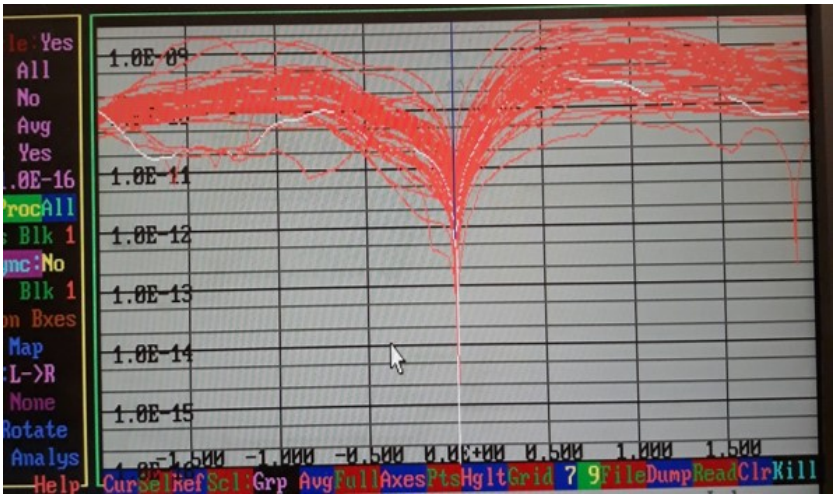

Figure 3.3: IV Spectra of Au(111) Surface Shown in Fig.3.2 on Semi-log Plot

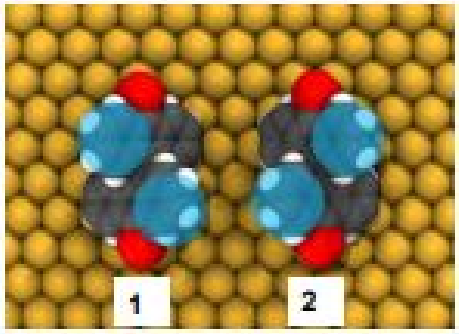

Figure 3.4: DBBA-on-surface Proposed Enantiomer Structures [8]

should be easily distinguishable from the DBBA and surface due to their spectra and data collected in this section.

3.2 DBBA Polymerization

Once the DBBA DCT has occurred, scanning voltages were limited to negative values. The number of contaminants on the surface dramatically increased after DCT. These contaminants are likely fiberglass particles or any other solvent particles that remained through applicator degassing. Since DBBA is formed by a C-C bond between two anthracene units and a C-Br bond at the opposite poles, it is not a planar molecule. Fig.3.4 shows the proposed orientations that DBBA may take on surfaces; red spheres represent Bromine, grey spheres represent Carbon, white spheres represent Hydrogen, and the blue circle indicates the highest point of each anthracene unit relative to the surface. Although these two orientations are equivalent given a 180° rotation, they are, when confined to the surface, enantiomers. Should these two enantiomers align next to each other, there may be an extra energy barrier associated with forcing them to align.

At room temperature, scans show that, rather than spread out on the Au(111) surface and separate from neighboring DBBA molecules, DBBA preferentially forms into monolayer 'islands'. No scans clearly indicated the existence of bilayers or trilayers of DBBA, implying that at room temperature the energy barrier for DBBA to diffuse around the surface is lower than the energy required to support stacking of DBBA.

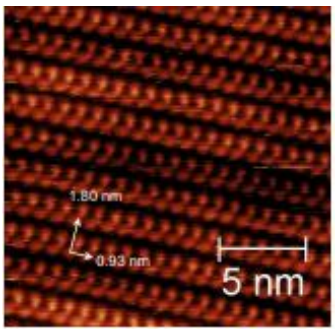

Figure 3.5: STM Image of Columnar Zigzag Structure of DBBA on Au(111), at -2V and 10pA [8]

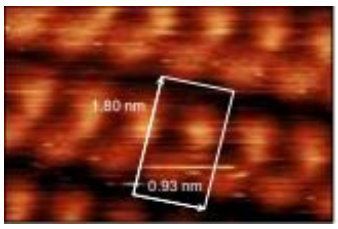

Figure 3.6: Zoomed in Fig. 3.5 at -2V and 10pA [8]

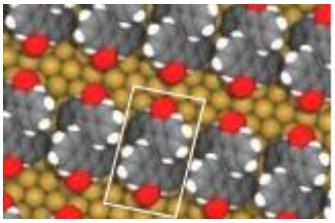

Figure 3.7: Proposed Structure of Fig. 3.6 [8]

The structure that DBBA islands appear to make on the Au(111) surface are referred to as a columnar zigzag structure and are shown in Figures 3.5, 3.6, and 3.7[8]. In these figures we can see that the proposed columnar zigzag structure has a unit cell consisting of a single DBBA molecule. This unit cell is boxed in Figures 3.6 and 3.7 and has dimensions of 1.80nm x 0.93nm. It is important to note that while two DBBA enantiomers are possible on the surface, the columnar zigzag structure seems to be entirely composed of a single kind of enantiomer. When this sample is then annealed at 100°C for 20mins, the structure rearranges and forms what is referred to as a close-packed zigzag structure. The close-packed zigzag structure has a much higher density of DBBA molecules, fitting 4 molecules in a 2.9nm x 1.6nm unit cell. This is shown in Figures 3.8, 3.9, and 3.10.

This close-packed zigzag structure was then scanned at alternating ±2V. -2V scans were used to images the surface as this voltage is not enough to perturb the DBBA. +2V scans are used to attempt polymerization of the DBBA. The results of these scans are shown in Figure 3.11. It is important to note that PA did not form after a single scan at +2V. Interestingly, the intermediate structure in between the DBBA island and PA chains is blurred and the scan at -2V cannot be resolved. Regardless, after two scans at +2V, multiple PA chains can be observed, each with length ≥5nm.

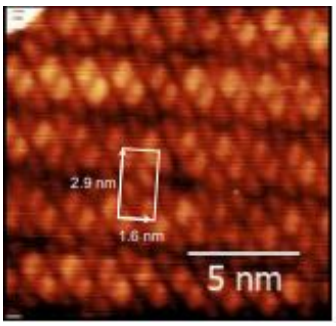

Figure 3.8: STM Image of Close-packed Zigzag Structure of DBBA on Au(111), at -2V and 10pA [8]

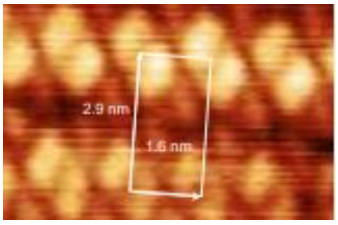

Figure 3.9: Zoomed in Fig. 3.8 at -2V and 10pA [8]

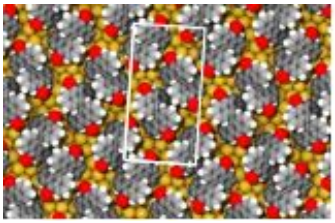

Figure 3.10: Proposed structure of Fig. 3.9 [8]

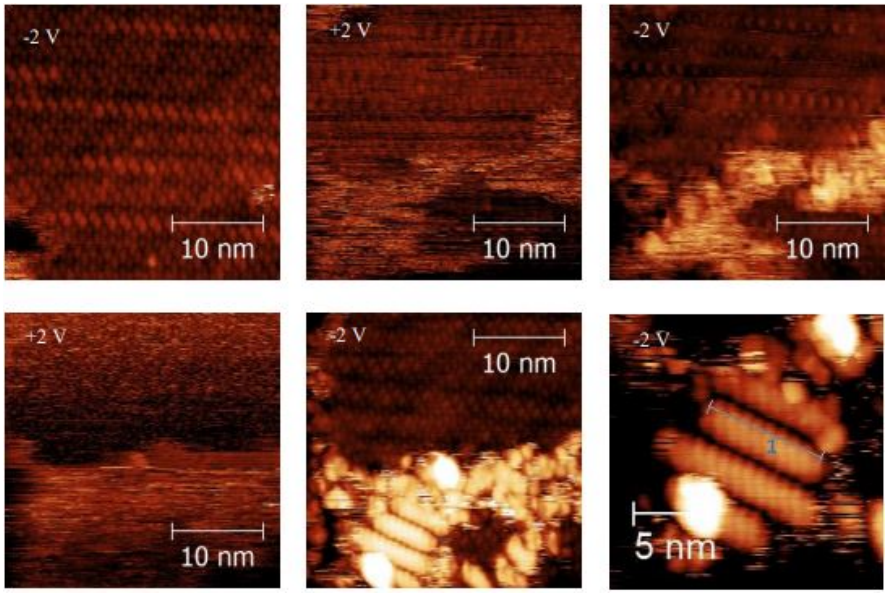

Figure 3.11: Alternating ±2V 10pA STM Scans of Close-packed Zigzag DBBA Island and Zoom-in on PA Structure [8]

CHAPTER 4

CONCLUSION

Through this experiment, an STM-tip has been shown to be capable of polymerizing DBBA monolayers on Au(111) substrates through electron-tunneling induced Ullmann coupling. It has also confirmed that the structure of monolayer DBBA varies with surface temperature. These results suggest that, at sufficient biases, STM should be capable of polymerizing other bromoaromatic monomers when these monomers are arranged in monolayers. This would allow for the selective debromination of precursors for many different types of GNR structures. Theoretically, this can also be extended to the creation of GNR heterostructures by polymerizing neighboring precursors of different GNR types. Further study into the possibility of selective cyclodehydrogenation of polymer chains into GNRs can be conducted in the future. This feat would solve the main issues currently facing GNR synthesis: uncontrollable length, uncontrollable spacing, and uncontrollable orientation. Additionally, future work could be done in performing the same experiment on a semiconducting or insulating substrate. Successfully completing this would allow for construction and use of GNR devices without current leakage though the substrate. Overall, the results of this experiment open the flood gates to a plethora of novel experiments that could lead to the highly controllable synthesis of GNRs and GNR devices.

REFERENCES

[1] J. Lyding, T. Shen, J. Hubacek, J. Tucker, and G. Abeln, "Nanoscale patterning and oxidation of h-passivated si(100)-21 surfaces with an ultrahigh vacuum scanning tunneling microscope," *Applied Physics Letters*, vol. 64(15), 1994.

[2] P. Albrecht and J. Lyding, "Ultrahigh-vacuum scanning tunneling microscopy and spectroscopy of single-walled carbon nanotubes on hydrogen-passivated si(100) surfaces." *Applied Physics Letters*, vol. 83(24):5029, 2003.

[3] S. B. Desai, S. R. Madhvapathy, A. B. Sachid, J. P. Llinas, Q. Wang, G. H. Ahn, G. Pitner, M. J. Kim, J. Bokor, C. Hu, H.-S. P. Wong, and A. Javey, "Mos2 transistors with 1-nanometer gate lengths," *Science*, vol. 354(6308), pp. 99–102, 2016.

[4] L. Chen, L. Wang, and D. Beljonne, "Designing coved graphene nanoribbons with charge carrier mobility approaching that of graphene," *Carbon*, vol. 77, pp. 868–879, 2014.

[5] J. Cai, P. Ruffieux, R. Jaafar, M. Bieri, S. B. T. Braun, M. Muoth, A. P. Seitsonen, M. Saleh, X. Feng, K. Mullen, and R. Fasel, "Atomically precise bottom-up fabrication of graphene nanoribbons," *Nature*, vol. 466(7305), pp. 470–473, 2010.

[6] J. Cai, K. Mullen, and R. Fasel, "Graphene nanoribbon heterojunctions," *Nature Nanotechnology*, vol. 9, pp. 869–900, 2014.

[7] J. Bjrk, "Reaction mechanisms for on-surface synthesis of covalent nanostructures," *Journal of Physics Condensed Matter*, vol. 28, p. 083002, 02 2016.

[8] A. Radocea, "Scanning tunneling microscopy investigation of atomically precise graphene nanoribbons," Ph.D. dissertation, University of Illinois Urbana-Champaign, 2017.